Intrinsic Negative Mass from Nonlinearity

F. Di Mei,[1,2] P. Caramazza,[1] D. Pierangeli,[1] G. Di Domenico,[1,2] H. Ilan,[3] A. J. Agranat,[3] P. Di Porto,[1] and E. DelRe[1,4,*]
[1]Dipartimento di Fisica, Università di Roma "La Sapienza," 00185 Rome, Italy
[2]Center for Life Nanoscience@Sapienza, Istituto Italiano di Tecnologia, 00161 Rome, Italy
[3]Applied Physics Department, Hebrew University of Jerusalem, 91904 Jerusalem, Israel
[4]ISC-CNR, Università di Roma "La Sapienza," 00185 Rome, Italy
(Received 17 November 2015; published 14 April 2016)

We propose and provide experimental evidence of a mechanism able to support negative intrinsic effective mass. The idea is to use a shape-sensitive nonlinearity to change the sign of the mass in the leading linear propagation equation. Intrinsic negative-mass dynamics is reported for light beams in a ferroelectric crystal substrate, where the diffusive photorefractive nonlinearity leads to a negative-mass Schrödinger equation. The signature of inverted dynamics is the observation of beams repelled from strongly guiding integrated waveguides irrespective of wavelength and intensity and suggests shape-sensitive nonlinearity as a basic mechanism leading to intrinsic negative mass.

DOI: 10.1103/PhysRevLett.116.153902

A negative energy density is thought to play a key role in cosmological conjectures, such as in stabilizing space-time wormholes and in explaining the supposed acceleration of the expanding Universe. At present, there is no proposed mechanism to support negative mass as a local space-time property. We here describe a mechanism able to support intrinsic negative mass through nonlinearity and provide experimental evidence of inverted dynamics for a light beam in a nanodisordered lithium-enriched potassium-tantalate-niobate (KTN:Li) crystal waveguide. The effect does not involve periodicity and, being intrinsic to the beam, is not limited to specific directions or energies.

Negative-mass particles should be repelled from attractive potentials and attracted by repelling ones, an unfathomed physics that could revolutionize our picture of nature, rendering abstract conjectures, such as space-time wormholes, stable (at least in principle) [1,2]. With a mass $m < 0$, the particle subject to a potential U suffers a force $F = -\nabla U$ but manifests the inverted acceleration $a = \nabla U/|m|$ (Fig. 1). Although all known particles have a positive or zero mass, conditions can be found in which the interaction of a particle with its environment leads to an effective mass $m^* \neq m$ that can, in specific conditions, also be negative. To date, $m^* < 0$ has been demonstrated in periodic systems [3–7], where the periodicity in the $\epsilon(k)$ band structure causes there to be a finite region of wave vectors for which the Bloch modes have a constant negative $d^2\epsilon/dk^2 < 0$, and with it a behavior described by a negative effective mass $m^* = \hbar^2(d^2\epsilon/dk^2)^{-1} < 0$ [8]. Intuitively, internal components move out of phase with respect to the global resonance of the system and lead to a negative-momentum response for a positive-momentum excitation [9]. Negative mass in these periodic systems is not intrinsic to the particle or wave, but only occurs for precise wave vectors at the edge of the Brillouin zone. At present, no mechanism has been proposed or demonstrated to be able to support negative mass as a property of a localized wave with inverted dynamics irrespective of particle energy or wave vector.

Consider the Schrödinger equation

$$[i\partial_t + (\hbar/2m)\nabla^2]\psi = (V/\hbar)\psi, \tag{1}$$

where $m > 0$. As an axiom, the SE is linear, but assume that there is some mechanism that violates this linearity so that, in general, the potential has two components: $V + V_{\mathrm{nl}}$, with V just a standard potential and V_{nl} a specific form of self-action. Indeed, although nonlinearity is absent in quantum mechanics, it is naturally built into the Einstein equations for which negative mass may have some important role. If V_{nl} is a small local perturbation associated to $|\psi|^2$, such as a Kerr effect with $V_{\mathrm{nl}} \propto |\psi|^2$, the SE turns into a nonlinear Schrödinger equation that supports solitons and rogue

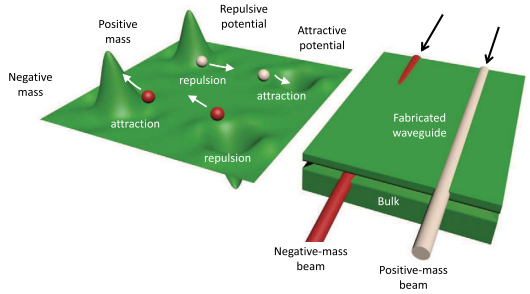

FIG. 1. Intrinsic inverted dynamics and a negative-mass Schrödinger equation (SE). (Left) In contrast to a positive-mass particle (lightly shaded sphere), a negative-mass particle (dark sphere) will be attracted by a repelling potential and repelled by a binding one. (Right) A propagating light beam described by a positive-mass SE (lightly shaded beam) will be guided by an integrated waveguide whereas a negative-mass light beam (dark beam) will be repelled by it and scattered into the bulk of the substrate.

waves, but for which no negative-mass dynamics emerges. Nonlinearity, in turn, can take many forms and can also be nonlocal, involving integrals and derivatives of $|\psi|^2$. If self-action is approximated by $V_{\rm nl}\psi \simeq (\hbar/2m')\nabla^2\psi$, then this will radically transform Eq. (1) into

$$[i\partial_t + (\hbar/2m^*)\nabla^2]\psi = (V/\hbar)\psi \tag{2}$$

that, when $m' < m$, corresponds to a negative-mass SE with $m^* = mm'/(m'-m) < 0$.

In our experiments we observe inverted dynamics in the propagation of light in a nanodisordered ferroelectric with the combined effect of an integrated slab waveguide and diffusive photorefractive nonlinearity [10–12]. Paraxial propagation along the z axis is governed by the parabolic equation

$$[i\partial_z + (1/2k)\nabla_\perp^2]A = -(k\Delta n/n_0)A, \tag{3}$$

where $k = k_0 n_0$, $k_0 = 2\pi/\lambda$, λ is the optical wavelength ($\omega = 2\pi c/\lambda$), n_0 is the unperturbed material index of refraction, A is the slowly varying optical field, and the local index of refraction is $n = n_0 + \Delta n$. Equation (3) maps into the 2 + 1D version of the SE of Eq. (2) for $t \equiv z/c$, $\psi \equiv A$, $m^* \equiv \hbar k/c$, and $V \equiv -\hbar c(k\Delta n/n_0)$. Hence, the causal relationship between the index of the refraction pattern and the paraxial propagation of a light beam is equivalent to that of a particle with finite energy in an appropriate potential. In other words, although photons have no mass, the description of a light field inside an inhomogeneous transparent material naturally leads to the introduction of $m^* \neq 0$.

In our case, the index modulation has two distinct components: $\Delta n = \delta n_{\rm nl} + \delta n$, where $\delta n_{\rm nl}$ is the diffusive nonlinear response caused by the propagating light, and $\delta n(\mathbf{r})$, the index modulation of the fabricated slab waveguide. The diffusive nonlinearity is associated to the electro-optic response $\delta n_{\rm nl} = -(n_0^3/2)g\epsilon_0^2\chi_{\rm PNR}^2|\mathbf{E}_{dc}|^2$ to the optically induced space-charge field $\mathbf{E}_{\rm dc}$, where g is the quadratic electro-optic coefficient, ε_0 is the vacuum dielectric permittivity, and $\chi_{\rm PNR}$ is the low-frequency susceptibility of the polar nanoregions (PNRs) [13,14]. With no external bias, photoexcited charge diffusion causes $\mathbf{E}_{\rm dc} = -(k_B T/q)\nabla I/I$, where k_B is the Boltzmann constant, T the crystal temperature, q the elementary charge, and $I = |A|^2$ is the intensity of the optical field A. The propagation equation now reads [11,12]

$$\left(i\partial_z + \frac{1}{2k}\nabla_\perp^2\right)A = -\frac{k\delta n}{n_0}A + \frac{1}{2k}\frac{L^2}{4\lambda^2}\left(\frac{\nabla_\perp I}{I}\right)^2 A, \tag{4}$$

where $L = 4\pi n_0^2\epsilon_0\sqrt{g}\chi_{\rm PNR}(k_B T/q)$, that, for Gaussian-like beams, is well approximated by the linear wave equation

$$[i\partial_z + (1/2k)(1 - L^2/\lambda^2)\nabla_\perp^2]A = -(k\delta n/n_0)A. \tag{5}$$

For $L > \lambda$, Eq. (5) maps to the 2 + 1D version of the SE of Eq. (2) with

$$m^* = -\frac{\hbar k}{c}\frac{1}{L^2/\lambda^2 - 1} < 0. \tag{6}$$

The $m^* < 0$ regime is here a product of nonlinearity, is localized around the beam, and is not limited to specific wavelengths, directions, or resonances of the system. We note that the passage from the nonlinear Eq. (4) to the linear Eq. (5) is rigorously valid only for Gaussian beams for which the peak intensity factors out of the term $(\nabla_\perp I/I)$. Consistently, even though beams may be spreading or becoming tighter during propagation, they will have only one specific value of m^* [as per Eq. (6)]. Because the passage to Eq. (5) is valid for Gaussian beam shapes, it follows that the effective negative mass will arise only if the δn is comparable or larger to the Gaussian beam itself. Fabricated waveguides considerably smaller than the beam waist will correspond to a potential well, as in Fig. 1, that is smaller than the size of the particle itself and will not necessarily lead to inverted dynamics. A flag to this spatial requirement is that Eq. (4) is spatially nonlocal whereas Eq. (5) is not.

We carry out experiments with the setup illustrated in Fig. 2(a). An x-polarized $\rm TEM_{00}$ beam from a He-Ne laser with ($\lambda_1 = 633$ nm) or from a doubled Nd:YAG laser ($\lambda_2 = 532$ nm) is first expanded and subsequently focused down onto the input facet of a sample of potassium-lithium-tantalate-niobate doped with copper (KLTN:Cu) crystal with a layer of He^+ ions implanted beneath its surface. The crystal is grown by the top-seeding solution growth method [15]. Its composition is determined by electron microprobe

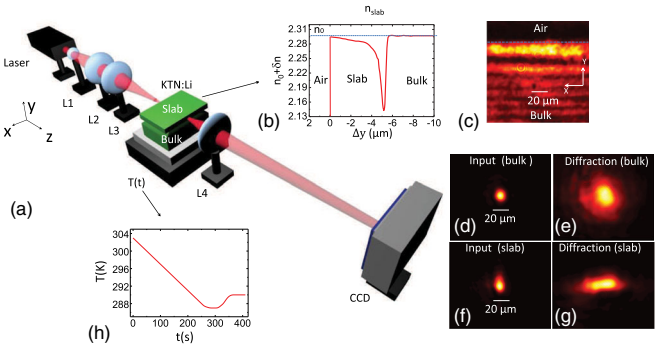

FIG. 2. Experimental setup, materials, and protocol. (a) A laser beam is launched into the KTN:Li waveguide and imaged on a CCD using lenses L1–L4 (L4 has NA ≃ 0.35). (b) Waveguide index profile (for 532 nm). (c) Typical graded waveguide output intensity distribution for an expanded plane-wave input. (d)–(g) Input and diffraction intensity distribution pattern in the bulk crystal and in the waveguide ($L/\lambda \simeq 0$). At a constant $T_A = 303$ K, the 100-μW input beam (waist $w_{0x} \sim w_{0y} = 8$ μm) (d) diffracts to 22 μm (e) after propagating a distance of $L_z \simeq 2.4$ mm through the bulk crystal. In the waveguide, the input beam (f) diffracts to $w_{0x} = 9.8$ μm and $w_{0y} = 31.7$ μm (g). (h) Supercooling protocol $T(t)$ to achieve $L/\lambda > 1$.

analysis and is found to be $K_{0.985}Li_{0.015}Ta_{0.63}Nb_{0.37}O_3$. The copper concentration is determined by inductively coupled plasma mass spectrometry and is found to be 68 ppm (in weight). A sample of $3.9^{(x)} \times 0.9^{(y)} \times 2.4^{(z)}$ mm^3 in size is cut along the [001] crystallographic axis. The ferroelectric phase transition of the sample is derived from dielectric measurements, and is found to be at $T_c = 285$ K. At the operating temperature range of 286–305 K the sample maintains high optical quality with refractive index of $n_0 = 2.3$, and quadratic electro-optic coefficient $g = 0.14$ m^4 C^{-2}. The He^+ ions are implanted at 2.3 MeV with fluence of 0.8×10^{16} ions/cm^2, which yields a partially amorphous layer with refractive index distribution as presented in Fig. 2(b) [16,17]. This forms a slab waveguide between the surface of the sample and the implanted layer that acts as the cladding [16]. The transverse intensity distribution of the beam is imaged using a CCD camera through the imaging lens. The diffraction pattern at the output facet of the crystal with $L/\lambda \simeq 0$, in the bulk and in the slab waveguide, respectively, is shown in Figs. 2(d)–2(g). In Fig. 2(h) we report the thermal shock protocol $T(t)$ near the peak in the dielectric response at $T_m = 287.5$ K [18–21] that allows a transient $L/\lambda > 1$. In practice, the crystal is first cleaned of photorefractive space charge by illuminating it with a microscope illuminator. Using a temperature controller that drives the current of a Peltier junction placed directly below the crystal in the y direction, we bring the sample to thermalize at $T_A = 303$ K. The sample is then cooled at the rate of 0.06 K/s to a temperature $T_D = 287$ K, where it is kept for 60 s. It is then reheated at a rate of 0.1 K/s to the operating temperature ($> T_D$) $T_B = 290$ K. The Peltier junction is placed below the sample so that during the process the crystal, exposed to ambient air (at ~290 K), experiences a transient temperature gradient along the y axis. Once T_B is reached and the temperature cycle $T(t)$ is complete, we switch on the laser beam, recording front view images of the intensity distribution.

In Fig. 3(a) we report the basic signature of intrinsic negative-mass SE dynamics: a beam expelled from the fabricated waveguide and scattered into the substrate. The beam is launched into the waveguide at $t = 0$ after the sample has undergone supercooling [the $T(t)$ in Fig. 2(h)]. It is first observed to focus down, to antidiffract, and then to suffer a strong repulsion, when it is scattered into the metastable bulk. Ultimately, the beam is observed to relax back into a linear diffraction, diffracting in the x direction and guided in the y. The sequence of events is further detailed in Fig. 3(b), where the beam peak intensity is plotted versus time. For comparison, we include the same curve when the same beam is launched into the bulk of the substrate. In the slab the beam suffers a transient scattering, whereas in the bulk it suffers antidiffraction dynamics [22,23]. The connection between this transient repulsion from the waveguide and the change in sign of the beam

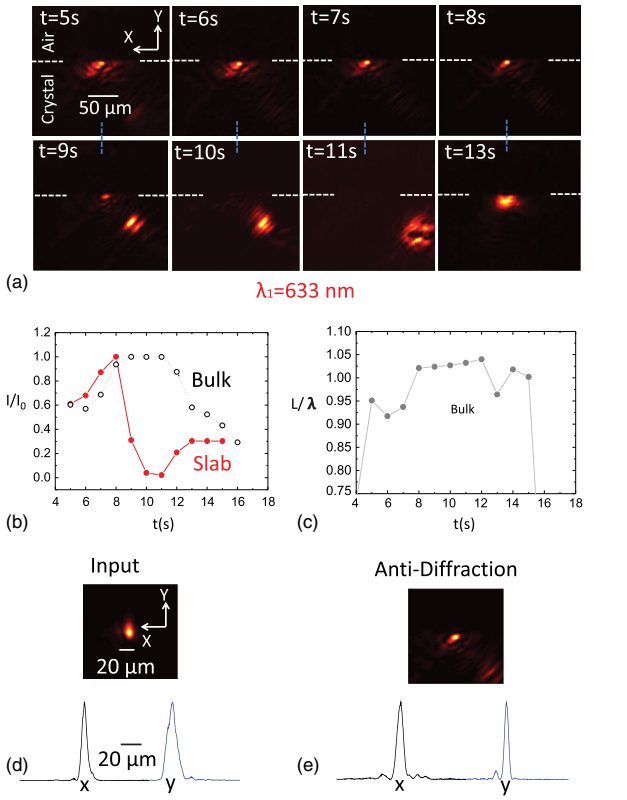

FIG. 3. A fabricated waveguide repels light as it acquires an intrinsic negative mass. (a) Time sequence of the output intensity distributions for $\lambda_1 = 633$ nm. (b) Comparison between the maximum peak intensity of the beam in the waveguide and in the bulk during the transient. (c) Time dependence of the L/λ in bulk. (d)–(e) Transient antidiffraction in the waveguide: the input beam (waist $w_{0x} = 9.9$ μm, $w_{0y} = 9.3$ μm) (d) and the output beam (minimum $w_{0x} = 6.8$ μm, $w_{0y} = 7.1$ μm, $L/\lambda \simeq 1.05$) during the aftershock (e).

mass in the equivalent SE is investigated in Fig. 3(c). Using the bulk antidiffraction and the analytical antidiffraction theory, L/λ as a function of time is evaluated. As expected, the instants of time during which the dipolar relaxation leads to $L/\lambda > 1$ coincide with the repulsive regime. In other words, the behavior of the light beam is drastically different between the guided and bulk conditions, as shown in Fig. 3(b); in one case it leads to a strong repulsion and scattering, and in the other to strong spatial localization. The intensity distribution of input and antidiffracting light corresponding to the $L/\lambda > 1$ stage before light is repelled by the waveguide as reported in Figs. 3(d)–3(e).

To validate the negative-mass SE model of Eq. (5) we repeated experiments for different intensities. The strong transient response reported in Figs. 3 and 4 has a characteristic response time of tens of seconds. Experiments using beams with different powers (10, 20, 40, 80, and 100 μW) lead to similar results and time scales. This approximate intensity-independent nature of the phenomenon is compatible with the overall linear nature of the effect as described in Eq. (2). Weak dependence of time scales on

peak intensity indicates that time dynamics are principally associated to the relaxation of the metastable PNR state, while the photorefractive buildup is relatively faster and the space-charge field can be considered at all times to be at steady state, corroborating the validity of the diffusive nonlinearity model. The value of the L parameter is estimated by measuring the output and input waist ratio.

To prove the effect is not limited to a specific region of wave vectors, in Fig. 4 we report beam repulsion for $\lambda = 532$ nm. The effect is analogous to the previous one, even though the details of the time evolution vary for each thermal shock, and only an average relaxation has a precise dynamical meaning. Specifically, the estimated value of L/λ in the two cases of Figs. 3 and 4 is comparable even though the thermal shock is the same and the wavelengths are different. Fluctuations are further exalted during the transition from the diffractive positive-mass SE to the antidiffractive negative-mass SE, as the waveguide goes from being guiding to antiguiding and allows light to explore its surroundings. An interesting difference in the dynamics of Figs. 3 and 4 is that the shorter wavelength case manifests a second focused stage reported in Fig. 4(e), displaced outside the original waveguide, where no second peak is found [Fig. 4(b)]. Specifically, the second peak is displaced approximately 4 μm in the y direction, inside the amorphous region [see Fig. 2(b)]. This indicates that the antiguiding amorphous layer becomes guiding in the negative-effective-mass regime. Unfortunately, the amorphous layer is only $\simeq 1$ μm wide and its effect on the beam cannot be fully described by the passage from Eq. (4) to Eq. (5). Congruently, for the longer-wavelength cases of Fig. 3, no analogous effect is observed.

Numerical simulations of the stationary full-nonlinear Eq. (4) are performed with a split-step Fourier method and

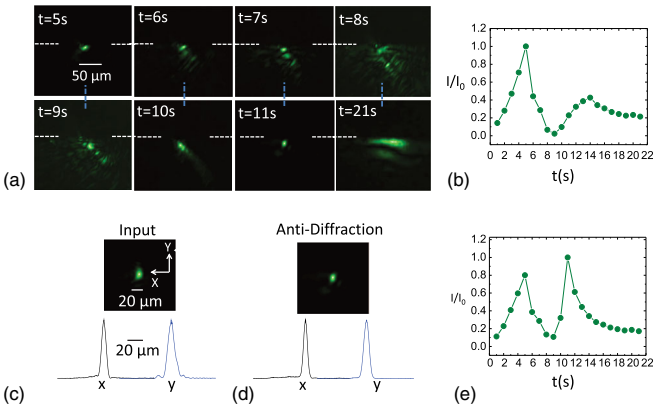

FIG. 4. Intrinsic negative-mass dynamics in the waveguide for $\lambda_2 = 532$ nm. (a) Time sequence of the output intensity distribution. (b) Maximum beam peak intensity in the waveguide during the transient. (c)–(d) Antidiffraction in the waveguide: (c) the input beam (waist $w_{0x} = 6.8$ μm, $w_{0y} = 9.9$ μm) and (d) the output beam during the aftershock (minimum beam width $w_{0x} = 7.1$ μm, $w_{0y} = 5.6$ μm, $L/\lambda \simeq 1.04$). (e) Maximum beam peak intensity of the output beam during the transient (see text).

with parameters matching our experimental conditions and slab-waveguide profile; results agree well with our observations and are reported in Fig. 5. They allow us to inspect the details of the propagation during evolution [Fig. 5(a)–5(d)] that cannot be directly detected optically and the resilience of the effect on distortions in the input Gaussian beam shape [Fig. 5(e)]. In particular, the transition from positive- to negative-mass dynamics is well reproduced as a function of (L/λ), with the expulsion of the beam from the waveguide to the substrate for $(L/\lambda) > 1$. We note that this expulsion is fundamentally different with respect to the phenomenon of soliton ejection and tunneling from a potential where the refractive-index well is modified by the nonlinear dynamics [24–26]. In our present phenomenon, no available nonlinearity could even marginally modify the huge fabricated index modulation (index modulations up to $\delta n \simeq 0.15$), and expulsion is a consequence of a change in the sign of the effective mass of the light beam.

Further supporting experiments on the role of the fabricated waveguide in the repulsion and scattering of the antidiffracting light beam and on the propagation of light during the ferroelectric-paraelectric phase-transition are reported in the Supplemental Material [27].

We have discussed how a shape-sensitive nonlinearity can lead to an intrinsic negative mass localized around a wave without the constraints associated with a periodic system or a resonance. We have shown an instance in which light-matter interaction, instead of modifying the nature of the propagation equation introducing nonlinear terms that alter wave propagation and lead to solitons, shock waves, and rogue waves [28–32], causes light to

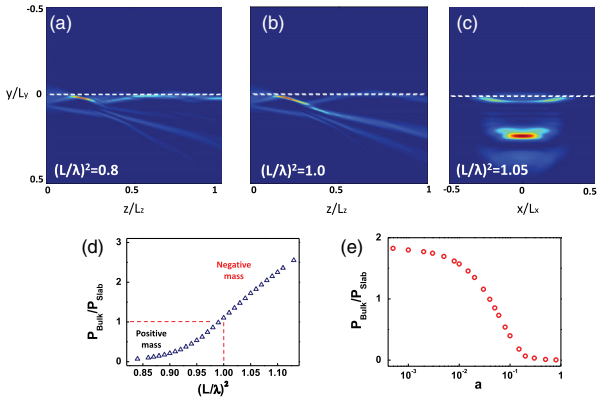

FIG. 5. Numerical simulation of Eq. (4). Dynamics of the beam along z ($L_x = 80$ μm, $L_z = 2.4$ mm, $\lambda = 633$ nm) (a) for $(L/\lambda)^2 = 0.85$ and (b) $(L/\lambda)^2 = 1.05$. (c) Output intensity distribution in the negative-effective-mass case. (d) Ratio of total power scattered into the bulk P_{Bulk} to that retained by the slab P_{Slab} versus $(L/\lambda)^2$. An effective positive mass is compatible with $P_{\mathrm{Bulk}}/P_{\mathrm{Slab}} < 1$, whereas a negative mass is compatible with inverted dynamics and $P_{\mathrm{Bulk}}/P_{\mathrm{Slab}} > 1$. (e) Dependence of inverted dynamics on beam shape: the $P_{\mathrm{Bulk}}/P_{\mathrm{Slab}}$ ratio for ever more distorted and squared-off Gaussian inputs ($\exp[-(x^2+y^2)/w_0^2) - a(x^4+y^4)/w_0^4]$, w_0 is the input beam width).

obey a modified linear propagation equation of the type $[i\partial_z - (1/2\tilde{k})\nabla_\perp^2]A = 0$, with $\tilde{k} > 0$. The effect hinges on a transient antidiffraction that is a product of nonlinearity and requires no underlying periodic pattern, in distinction to linear antidiffraction [33–36]. In these conditions, beam propagation naturally maps the dynamics of a negative-mass particle described by the Schrödinger equation with $m^* = -\hbar\tilde{k}/c < 0$, so that a fabricated waveguide with a strong guiding index modulation $\delta n/n \sim 10\%$, amounting to a strong binding potential, repels light instead of attracting it. In distinction to previous studies into negative mass, which focus on effective dynamics in periodic potentials, our study here demonstrates a local mechanism that provides negative mass compatible with basic negative-mass conjectures, such as those required to stabilize space-time wormholes.

The research leading to these results was supported by funding from Grant No. PRIN 2012BFNWZ2, and Sapienza 2014/2015 Projects. A. J. A. acknowledges the support of the Peter Brojde Center for Innovative Engineering.

*eugenio.delre@uniroma1.it

[1] M. S. Morris and K. S. Thorne, Wormholes in spacetime and their use for interstellar travel: A tool for teaching general relativity, Am. J. Phys. **56**, 395 (1988).

[2] M. S. Morris, K. S. Thorne, and U. Yurtsever, Wormholes, Time Machines, and the Weak Energy Condition, Phys. Rev. Lett. **61**, 1446 (1988).

[3] Z. Liu, X. Zhang, Y. Mao, Y. Y. Zhu, Z. Yang, C. T. Chan, and P. Sheng, Locally resonant sonic materials, Science **289**, 1734 (2000).

[4] H. Sakaguchi and B. A. Malomed, Dynamics of positive- and negative-mass solitons in optical lattices and inverted traps, J. Phys. B **37**, 1443 (2004).

[5] S. Yao, X. Zhou, and G. Hu, Experimental study on negative effective mass in a 1D mass spring system, New J. Phys. **10**, 043020 (2008).

[6] S. Batz and U. Peschel, Diametrically Driven Self-Accelerating Pulses in a Photonic Crystal Fiber, Phys. Rev. Lett. **110**, 193901 (2013).

[7] O. Firstenberg, T. Peyronel, Q. Y. Liang, A. V. Gorshkov, M. D. Lukin, and V. Vuletic, Attractive photons in a quantum nonlinear medium, Nature (London) **502**, 71 (2013).

[8] C. Kittel, *Introduction to Solid State Physics*, 8th ed. (John Wiley and Sons, New York, 2005).

[9] M. Wimmer, A. Regensburger, C. Bersch, M. A. Miri, S. Batz, G. Onishchukov, D. N. Christodoulides, and U. Peschel, Optical diametric drive acceleration through actionreaction symmetry breaking, Nat. Phys. **9**, 780 (2013).

[10] D. N. Christodoulides and T. H. Coskun, Diffraction-free planar beams in unbiased photorefractive media, Opt. Lett. **21**, 1460 (1996).

[11] B. Crosignani, E. DelRe, P. Di Porto, and A. Degasperis, Self-focusing and self-trapping in unbiased centrosymmetric photorefractive media, Opt. Lett. **23**, 912 (1998).

[12] E. DelRe, E. Spinozzi, A. J. Agranat, and C. Conti, Scale-free optics and diffractionless waves in nanodisordered ferroelectrics, Nat. Photonics **5**, 39 (2011).

[13] A. A. Bokov and Z.-G. Ye, Recent progress in relaxor ferroelectrics with perovskite structure, J. Mater. Sci. **41**, 31 (2006).

[14] A. Gumennik, Y. Kurzweil-Segev, and A. J. Agranat, Electrooptical effects in glass forming liquids of dipolar nano-clusters embedded in a paraelectric environment, Opt. Mater. Express **1**, 332 (2011).

[15] R. Hofmeister, S. Yagi, A. Yariv, and A. J. Agranat, Growth and characterization of KLTN:Cu,V photorefractive crystals, J. Cryst. Growth **131**, 486 (1993).

[16] A. Gumennik, A. J. Agranat, I. Shachar, and M. Hass, Thermal stability of a slab waveguide implemented by α particles implantation in KLTN, Appl. Phys. Lett. **87**, 251917 (2005).

[17] A. Gumennik, H. Ilan, R. Fathei, A. Israel, A. J. Agranat, I. Shachar, and M. Hass, Design methodology of refractive index engineering by high energy particles implantations in electrooptic materials, Appl. Opt. **46**, 4132 (2007).

[18] J. Parravicini, C. Conti, A. J. Agranat, and E. DelRe, Programming scale-free optics in disordered ferroelectrics, Opt. Lett. **37**, 2355 (2012).

[19] F. Di Mei, D. Pierangeli, J. Parravicini, C. Conti, A. J. Agranat, and E. DelRe, Observation of diffraction cancellation for nonparaxial beams in the scale-free-optics regime, Phys. Rev. A **92**, 013835 (2015).

[20] Y.-C. Chang, C. Wang, S. Yin, R. C. Hoffman, and A. G. Mott, Giant electro-optic effect in nanodisordered KTN crystals, Opt. Lett. **38**, 4574 (2013).

[21] Y.-C. Chang, C. Wang, S. Yin, R. C. Hoffman, and A. G. Mott, Kovacs effect enhanced broadband large field of view electro-optic modulators in nanodisordered KTN crystals, Opt. Express **21**, 17760 (2013).

[22] F. Di Mei, J. Parravicini, D. Pierangeli, C. Conti, A. J. Agranat, and E. DelRe, Anti-diffracting beams through the diffusive optical nonlinearity, Opt. Express **22**, 31434 (2014).

[23] E. DelRe, F. Di Mei, J. Parravicini, G. B. Parravicini, A. J. Agranat, and C. Conti, Subwavelength anti-diffracting beams propagating over more than 1,000 Rayleigh lengths, Nat. Photonics **9**, 228 (2015).

[24] Y. Linzon, R. Morandotti, M. Volatier, V. Aimez, R. Ares, and S. Bar-Ad, Nonlinear Scattering and Trapping by Local Photonic Potentials, Phys. Rev. Lett. **99**, 133901 (2007).

[25] A. Barak, O. Peleg, C. Stucchio, A. Soffer, and M. Segev, Observation of Soliton Tunneling Phenomena and Soliton Ejection, Phys. Rev. Lett. **100**, 153901 (2008).

[26] M. Peccianti, A. Dyadyusha, M. Kaczmarek, and G. Assanto, Escaping Solitons from a Trapping Potential, Phys. Rev. Lett. **101**, 153902 (2008).

[27] See Supplemental Material at http://link.aps.org/supplemental/10.1103/PhysRevLett.116.153902 for further supporting experiments.

[28] *Spatial Solitons*, edited by S. Trillo and W. Torruellas (Springer, Berlin, 2001).
[29] N. K. Efremidis and K. Hizanidis, Disordered Lattice Solitons, Phys. Rev. Lett. **101**, 143903 (2008).
[30] Z. Chen, M. Segev, and D. N. Christodoulides, Optical spatial solitons: Historical overview and recent advances, Rep. Prog. Phys. **75**, 086401 (2012).
[31] D. Pierangeli, F. Di Mei, C. Conti, A. J. Agranat, and E. DelRe, Spatial Rogue Waves in Photorefractive Ferroelectrics, Phys. Rev. Lett. **115**, 093901 (2015).
[32] D. Pierangeli, M. Flammini, F. Di Mei, J. Parravicini, C. E. M. de Oliveira, A. J. Agranat, and E. DelRe, Continuous Solitons in a Lattice Nonlinearity, Phys. Rev. Lett. **114**, 203901 (2015).
[33] H. Kosaka, T. Kawashima, A. Tomita, M. Notomi, T. Tamamura, T. Sato, and S. Kawakami, Self-collimating phenomena in photonic crystals, Appl. Phys. Lett. **74**, 1212 (1999).
[34] H. S. Eisenberg, Y. Silberberg, R. Morandotti, and J. S. Aitchison, Diffraction Management, Phys. Rev. Lett. **85**, 1863 (2000).
[35] K. Staliunas and R. Herrero, Nondiffractive propagation of light in photonic crystals, Phys. Rev. E **73**, 016601 (2006).
[36] O. Firstenberg, P. London, M. Shuker, A. Ron, and N. Davidson, Elimination, reversal and directional bias of optical diffraction, Nat. Phys. **5**, 665 (2009).